Effects of stitch density and stitch thread thickness on mode II delamination properties of Vectran stitched composites

J. Herwan*, A. Kondo, S. Morooka and N. Watanabe

Mode II delamination properties of Vectran stitched composites were investigated, and tabbed end notch flexural specimen testing was used to prevent premature failure. The effects of stitch density and stitch thread thickness were explored, and fibre compaction due to the stitching process was also verified. The results show that, in moderately stitched laminates (low stitch density), the improvement in G_{IIC} was negligible. Crack bridging by the stitch threads at the crack zone were mostly compensated for the effect of fibre compaction, which reduced the G_{IIC} values. Conversely, in densely stitched laminates (high stitch density), G_{IIC} values were improved significantly (2·4 times higher than those of unstitched laminates). The effects of stitch thread thickness appeared to be negligible in moderately stitched laminates. For densely stitched laminates, thicker stitch thread (500 denier) possessed G_{IIC} values that were 45·7% higher than thinner stitch thread (200 denier).

Keywords: CFRP, 3D reinforcement, Stitching, Delamination, Mode II, Interlaminar shear toughness

Introduction

In the last decade, use of carbon fibre reinforced polymers (CFRPs) in lightweight structures has increased significantly, especially in aerospace applications. For example, CFRPs make up more than 50% of the total weight of Boeing 787 and Airbus A350 XWB. In automotive applications, the use of CFRPs is rising in parallel with the manufacture of electric cars. Carbon fibre reinforced polymers comprise most of the internal structure and body of the BMW i3.

Although there are many advantages of using CFRPs, they are subject to interlaminar strength debilities that can cause delamination. To overcome the issue, three-dimensional (3D) fibre reinforced polymer composites have been developed since the mid-1980s.[1] The techniques for 3D reinforcement include braiding,[2,3] knitting,[3] weaving,[3–5] z-pinning[6] and stitching.[7] Stitching is one of the most promising methods. The existence of stitch threads in composite laminates increases mode I (opening mode) delamination through a stitch bridging mechanism and reduces the size of the crack propagation zone.[8–11] The mode I energy release rate in stitched laminates could reach 15 times that of unstitched laminates, depending on the type and diameter of the stitch thread, stitch density and stitch distribution.

Furthermore, in many real cases, such as in composite plates under low velocity impact, delamination propagates mainly via a mode II (shear mode) process.[12] The first experimental work on stitched composites undergoing mode II delamination was reported by Sankar and Sharma.[13] Kevlar and glass fibres were used as stitch threads in unidirectional CFRPs, and the existence of stitch threads increased the energy release rates G_{IIC} by between five and eight times. Generally, G_{IIC} values increased with increasing stitch density, except for Glass-750 stitch thread, where optimum stitch density was probably achieved at the level 2·48 stitches/cm^2. The area method with compliance of the unloading curve was applied to calculate G_{IIC}. Jain *et al.*[14] reported that the G_{IIC} values were improved by up to 3·3 times when Kevlar and carbon T-900 were used as stitch threads. Stitch density and stitch thread thickness did not affect G_{IIRi} (initial energy release rate) but had considerable effects on G_{IIRs} (steady state energy release rate). It was also reported that, in some specimens, compression failure occurred at the stitch lines closest to the central loading pin. To avoid premature failure, Wood *et al.*[15] used tabbed end notch flexural (TENF) specimens, embedding aluminium 2024 T3 sheets of 2 mm thickness at both the upper and lower surfaces of specimens. In their experiment, liquid crystal polymers (1500 denier) were stitched on satin weave carbon fibres with epoxy matrixes. They reported that the energy release rates of stitched composites were 2·25 times those of unstitched composites and were negligibly affected by stitch distribution.

Type of stitch thread has a significant effect on the properties of stitched composites. A previous study of our group on mode I interlaminar properties[16] concluded that Vectran has better reinforcement compared

Department of Aerospace Engineering, Tokyo Metropolitan University, 6-6 Asahigaoka, Hino-shi, Tokyo 191-0065, Japan

*Corresponding author, email jonny-herwan@ed.tmu.ac.jp

Published by Maney on behalf of the Institute
Received 22 August 2014; accepted 10 September 2014
DOI 10.1179/1743289814Y.0000000103

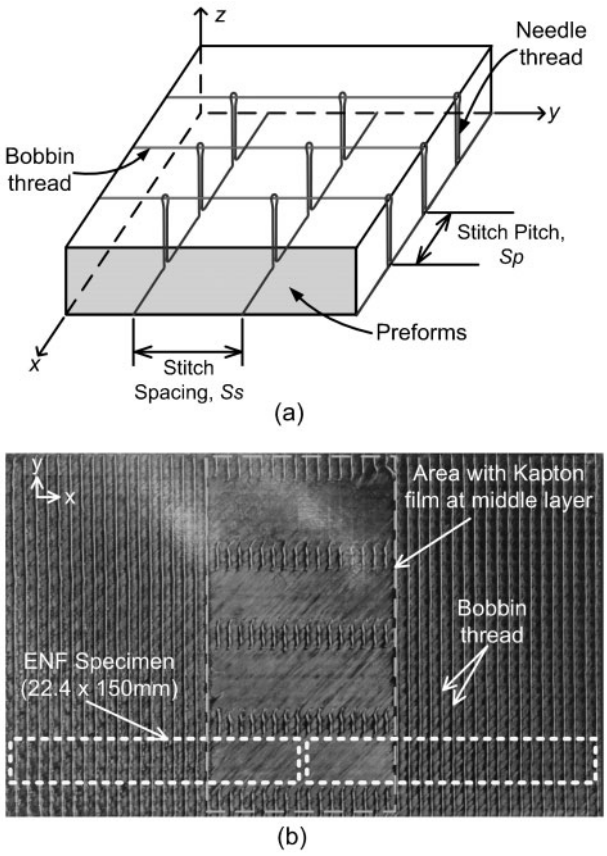

1 *a* modified lock stitching pattern and *b* 3×3 mm stitched composite laminate with ENF specimen cutting position

to Kevlar and carbon fibres. Additionally, Vectran also has a lower propensity to absorb moisture.

To the best of our knowledge, this article is the first to investigate the effects of stitch thread thickness and stitch density on mode II delamination properties of quasi-isotropic CFRP laminates with Vectran as the stitch thread. The work also proposes to complement the delamination behaviour of the same materials that have been reported by our group (on mode I delamination testing).[11,16] Furthermore, to enhance the analysis, the effects of fibre compaction during stitching processes have also been originally investigated.

Experimental methods

Material and sample preparation

Both unstitched and stitched composite laminates used in this test were made with T800SC-24K (Toray Industry) and follow the same lay-up as our group's previous work on mode I delamination testing[11] [24-ply quasi-isotropic $(+45/0/-45/90)_{3S}$]. Toyota Industries Corporation fabricated the stitched composite laminates using their patented modified lock stitching process.[17] Multidirectional stitched laminates prepared using this typical process exhibit minimal fibre waviness compared to unidirectional ones. The multidirectional preformed fibres can be stretched in many directions during the stitching process to restrain the fibre waviness. It is worth minimising the fibre waviness in mode II delamination test specimens because it affects the results by slip locking[18] and emerging mode I processes. Therefore, quasi-isotropic laminates were used in this experimental work.

To investigate the effect of stitch thread thickness, two fibre linear densities were used (200 and 500 denier, equal to 0·0158 and 0·0394 mm^2 cross-sectional areas respectively). Meanwhile, the effects of stitch density were evaluated by manufacturing different types of specimens: so called moderately and densely stitched laminates. Both types have different stitch spacing S_s and stitch pitch S_p, as illustrated in Fig. 1*a*. These moderately and densely stitched laminates had $S_s \times S_p$ values of 6 × 6 mm and 3 × 3 mm respectively. The stitch density *SD* of the laminates can be calculated using the following expression

$$SD = \frac{1}{S_s \times S_p} \quad (1)$$

Kapton film was inserted between the middle layers of the laminates to facilitate the initial crack, and stitching did not occur in the specimen area where the film was inserted (Fig. 1*b*).

After the stitching process, XNR/H6813 Denatite resin (Nagase Chemtex Corp.) was used to consolidate the composite laminates using a vacuum assisted resin transfer moulding technique. The same process was used to manufacture the unstitched laminates, but a wider area was left unstitched, so that the total thickness remained similar between the stitched and unstitched laminates. The average thickness of the laminate plates was 5·16 mm.

The specimens were cut from the plates using a water cooled cutting machine (AC-400CF, Maruto) and were 22·4 mm wide and 150 mm long. Five types of specimens were prepared (Table 1).

Test method

Until now, international consensus on the standard procedure of mode II delamination testing has not been achieved, even though collaborative work has been conducted by the European Structural Integrity Society,

Table 1 Types of test specimens

Specimen type	Unstitched	Stitched 6×6 200 denier	Stitched 6×6 500 denier	Stitched 3×3 200 denier	Stitched 3×3 500 denier
Code	Unstitched	6D2	6D5	3D2	3D5
Stitch pitch/mm	…	6	6	3	3
Stitch spacing/mm		6	6	3	3
Stitch density/cm^{-2}	…	2·78	2·78	11·11	11·11
Stitch thread thickness/denier	…	200	500	200	500
Fibre volume fraction/%	53·9	53·7	54·2	54·4	54·9
Number of needle thread lines in width direction	…	4	4	8	8
Number of specimens	6	6	6	6	6

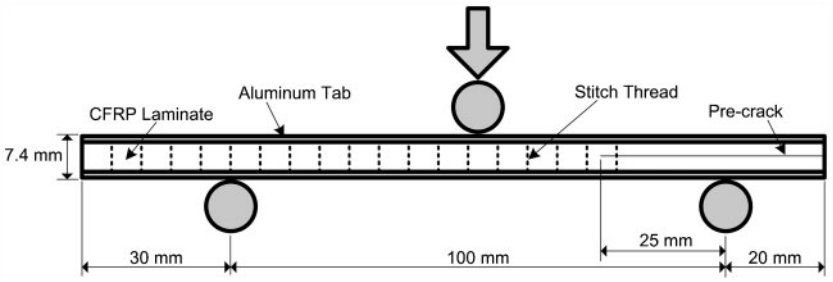

2 Tabbed end notch flexure (TENF) specimen set-up with specific crack tip position

Japan Industrial Standards (JIS) group and ASTM.[19] A review on prospective standard procedures has been reported by Brunner *et al.*[20] However, a local standard method already existed (Japanese Industrial Standard JIS K7086),[21] and a draft European Standard EN 6034 has been proposed.

In this experimental work, the ENF test adopted refers to JIS K7086, mainly for the test fixtures and specimen sizes. Modifications have been conducted to overcome many problems on stitched composites. Based on our preliminary test and those of many other reported works,[14,15] stitched composite laminates are prone to failure before crack propagation during ENF testing. To avoid this, aluminium tabs were embedded at the upper and bottom surfaces of the specimen using high strength epoxy (Hysol EA 9309·3NA from Henkel Corporation).[22] This type of epoxy contains 0·13 mm glass beads for bond line thickness control, so that the total thickness of TENF specimens can be kept constant at $7{\cdot}39 \pm 0{\cdot}03$ mm. In this work, Al-7075 T6 was selected as the tab material because it possesses the highest yield strength among the aluminium alloys. A relatively thin aluminium tab (thickness=1 mm) was also selected to minimise the shear stress at the interface between the composite laminate and aluminium tab so that delamination at the bonded joint could be avoided. A detailed description of the TENF specimen set-up is given in Fig. 2.

Additionally, the crack tip was developed using a precracking process. Precracks greatly influence the energy release rates of composite laminates.[23,24] They remove resin pockets at the ends of the inserted film. These resin pockets create a blunt crack tip and increase the crack's propagation resistance. Before ENF testing, a crack opening that was a few millimetres long was created using a sharp, thin razor blade. Then, three-point bend loading was used to propagate the crack to a position between 1 and 3 mm beyond the end of the Kapton film. This pre-ENF test was conducted with a half-span length of 40–45 mm, and the loading point was placed exactly in between the first and second stitch row. Because this pre-ENF test was conducted in the unstitched region, unstable crack propagation occurred and stopped exactly at the loading point. The greatest advantage of using this precracking process was that the crack tip position was located at the same region for all specimens (between the first and second stitch row), as shown in Fig. 2. Furthermore, to enhance the contrast of the crack tip, brittle white paint was applied to both edges of the specimens.

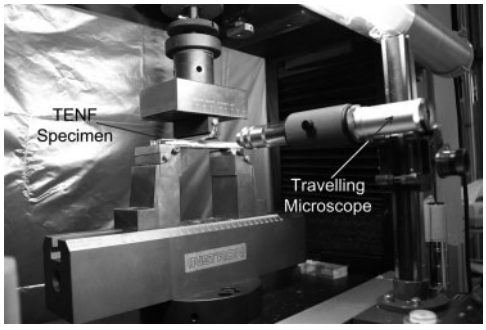

3 Mode II delamination test set-up

Subsequently, TENF tests were conducted using a 4505 series Instron machine with a 10 kN load cell over a total span of 100 mm (Fig. 3). The specimens were loaded at a constant crosshead speed of 0·5 mm min^{-1} until 1 kN was reached, then the crosshead speed was reduced to 0·1 mm min^{-1} to enable slow crack propagation. After unloading, the new crack length was measured using a travelling microscope at $\times 25$ magnification and 0·01 mm reading accuracy.

Data reduction

The energy release rate G_{II} was calculated using the compliance calibration method of Carlsson and Gillespie[23] and Carlsson *et al.*[25] This method was selected because it can accommodate tabs being on the specimen without any modifications to the basic G_{II} calculation.[26] The energy release rate can be evaluated by differentiation of compliances with respect to crack lengths when there is no plastic deformation and no damage except for interlaminar fracture. Before TENF testing, the specimen compliance was measured for five crack lengths (0, 10, 20, 30 and 40 mm) by applying small loadings until between 600 and 700 N was reached (0·1 mm min^{-1} crosshead speed). Similar procedures were repeated at each specific point where the energy release rate was being measured. Placement of the specimens was adjusted to obtain a new compliance data, depending on the available space. For example, to measure G_{IIC} at a typical crack length of 45 mm, the compliances were measured at crack tip positions of 37, 41, 45 and 49 mm from the right supporting pin. Then, compliance values were plotted in terms of C/Co versus $(a/L)^3$, and the slope m of the curve was measured.

Energy release rates were calculated as follows

$$G_{II} = \frac{3mP^2a^2Co}{2wL^3} \tag{2}$$

where Co is the compliance of the specimen without any crack along the span, a is the crack length and P is the peak load at which the crack starts to propagate. Parameters w and L are the width of the specimen and half-length of the span respectively. It is important to

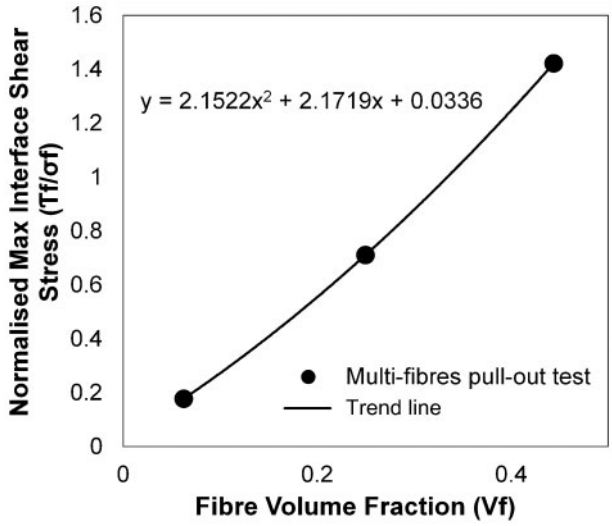

4 Plot showing normalised maximum interface shear stress at loaded fibres end of pullout test simulation (data from Fu *et al.*[32])

note that the slope m in equation (2) is specific for each crack length on the specimen to be tested.

To investigate the effects of stitch thread thickness and stitch density, G_{IIC} values were determined for crack lengths of 25 and 45 mm for all specimens. These crack lengths were close to the initial and steady state points given by Jain *et al.*[14] In the present work, steady states (flat portions of R curves) were not achieved in some type of specimens; therefore, a crack length of 45 mm was chosen. In between the two crack lengths, only one or two other G_{IIC} values could be measured for each specimen due to the limited space available. However, the R curve (G_{II} versus crack length) could still be determined for each type of specimen.

Measurement of local fibre volume fraction

This subtopic was added into the experimental work based on preliminary results of TENF tests and related references,[27,28] which raised queries about correlations between fibre volume fraction and G_{IIC} values. To address this issue, the explanation is separated as detailed in the following.

Fibre compaction due to stitching process

It has been reported that fibre compaction during the stitching process increased the local fibre volume fraction V_{fl} through numerous steps.[29] First, the insertion of the stitch fibre moves the preformed fibres laterally. The fibres between the two stitch lines are then deflected, causing a local increase in the volume fraction. Second, the tension forces created during the stitching process enhance fibre compaction. Finally, the pressure applied to stitched fibres during laminate consolidation also increases V_{fl}, especially in the area under the stitched threads. These three factors are inevitable characteristics of stitched composite laminates.[7]

Effect of local fibre volume fraction on energy release rate

The effects of V_{fl} on mode I and II delamination properties of five harness satin woven carbon fibre/epoxy resin composites have been investigated.[27] However, it was difficult to measure these effects in mode II delamination testing due to the serious influence of friction and interlocking between delamination

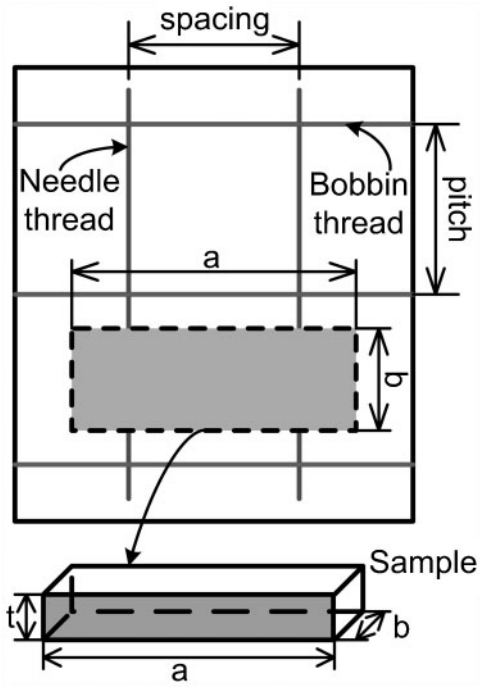

5 Schematic of cutting method used for sample burnoff tests

surfaces. Work on similar case was carried out by Feret *et al.*[28] using a mixed mode delamination test. They concluded that at the high mode II ratio, the total crack propagation energy was decreased by increasing V_{fl}.

The above reported works used fabric/woven carbon fibres. To enhance the hypothesis on non-fabric composites, a mode II static fracture mechanism may be the best approach. Hojo *et al.*[30] reported that, during static ENF testing, microcracks initiated first at the fibre/matrix interfaces, followed by matrix cracking between the fibres. These microcracks appeared when the shear stress at the fibre/matrix interface near the crack tip reached a certain value (called the critical shear stress).[31] Furthermore, in relation to the maximum shear stress at fibre/matrix interfaces, multifibres pullout study at different V_{fl} (Ref. 32) was adopted. Quantitatively, this numerical study explained that the maximum shear stress at the interface will increase with increasing V_{fl}, following the curve shown in Fig. 4.

Measurement method of local fibre volume fraction

JIS K7075-1991[33] was referred to when conducting burnoff tests to measure fibre volume fraction. The measurement was performed as follows:

(i) the sample mass was measured
(ii) the sample was burned with a gas torch
(iii) the mass of the burned sample was remeasured
(iv) the fibre volume fraction was calculated.

Before burning, the masses of each specimen were measured in open air and under water so that the densities of the samples could be calculated.

To measure local volume fraction at the position where it increases as a result of the stitching process, the specimens were cut as shown in Fig. 5. This cutting position mostly excluded the resin rich region, and the three main factors related to fibre compaction (discussed above) were encountered. For the stitched laminates of

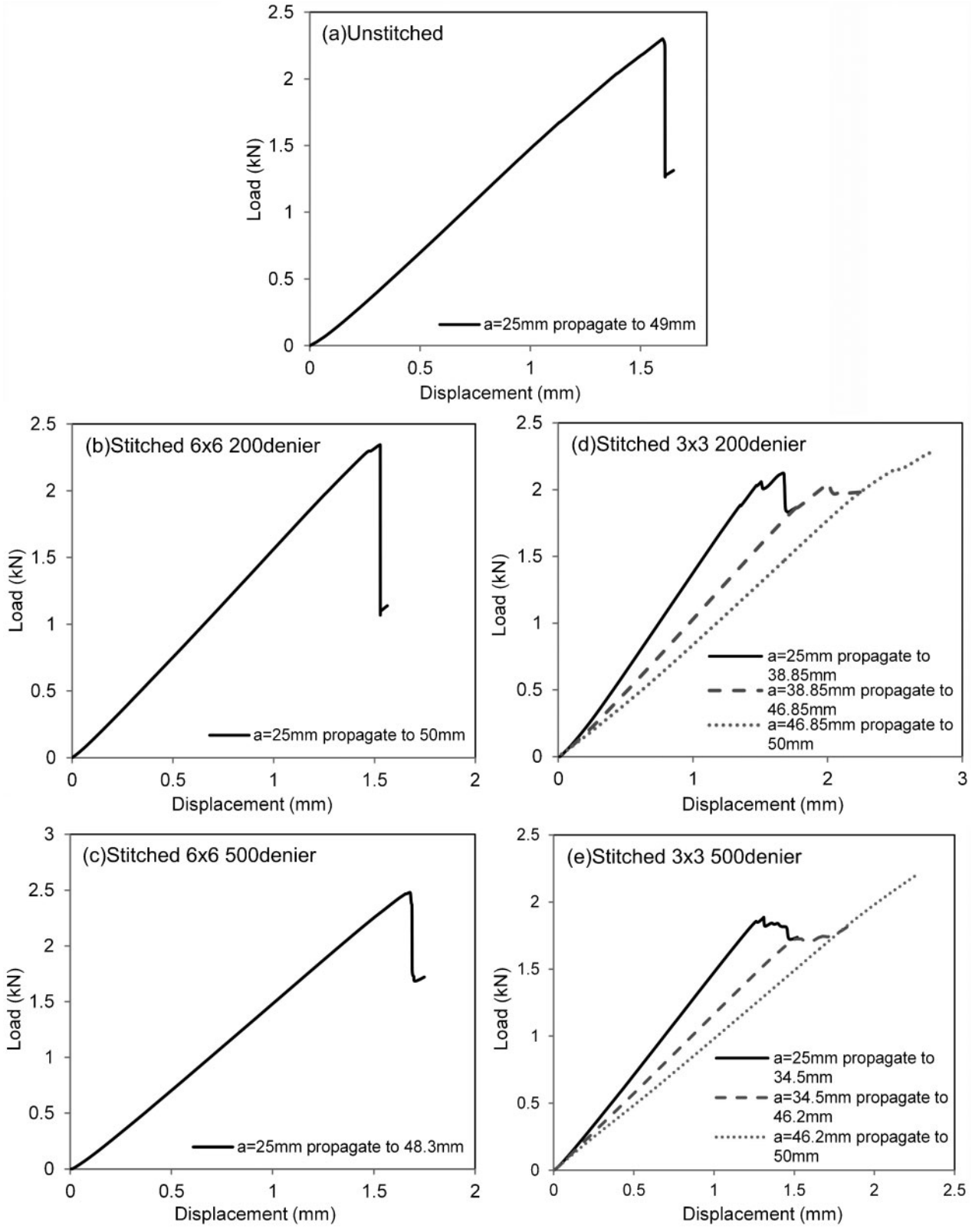

6 Typical load–displacement curves for unstitched and stitched specimens

6×6 mm, the length a and width b were 10 and 4 mm respectively. For the unstitched and stitched laminates of 3×3 mm, the dimensions were 10×2 mm. After cutting was complete and before the burnoff tests, the remaining needle thread was sanded off using emery paper. The average thickness t of all specimens was 4·88 mm. Five to six burnoff specimens from each type of laminate were investigated.

Results and discussion

Load–displacement curves

Typical load–displacement curves for all types of specimens that resulted from TENF tests are displayed in Fig. 6. In the case of unstitched and moderately stitched specimens, it is evident in Fig. 6*a–c* that the cracks suddenly propagated to the centre of the loading pin.

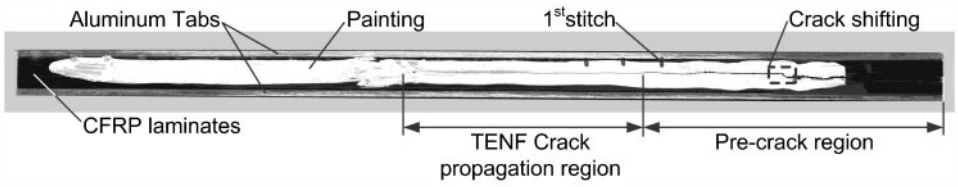

7 Tested specimen of stitched 6 × 6 mm and 500 denier thread thickness

The densely stitched laminates (Fig. 6*d and e*) could detain crack propagation, and their load–displacement curves consist of two or three steps until the cracks reach the centre of the loading pin.

After completion of the TENF tests, all specimens were visually inspected to determine whether any plastic deformation of the specimens or delamination occurred at the interfaces between the composite laminates and the aluminium tabs. Neither plastic deformation nor delamination was observed (Fig. 7), guaranteeing that the energy lost during the tests was only due to interlaminar crack extension.

Additionally, Fig. 7 also reveals that the crack shifted from the centre (between the 90/90° layer) to the interface between the −45/0° layer. This occurred during the precracking process, which used either a sharp razor blade (at the beginning) or the three-point bending fixture, as described previously. This behaviour appeared on all types of specimens as demonstrated in Fig. 8. Other researchers have also reported that cracks shift to the closest 0° layer on the compressive side.[34–36]

During the TENF tests, the cracks propagated at the interface between −45/0° layers without crack shifting (Figs. 7 and 8). Some comparison studies have been proposed to address these issues. Polaha *et al.*[36] investigated carbon/epoxy laminates with θ/−θ delaminated interfaces where θ=0, 15 and 30°. They concluded that the effect of θ on G_{IIC} was negligible. However, De Morais[37] conducted numerical analysis on several multidirectional laminates and reported that, in the case of the 0/45° delamination interface, mode III and I processes arose by 3 and 1% of the total energy release rate respectively. Additionally, related to asymmetry crack plane, Mollón *et al.*[38] concluded that it has no significant effects on G_{II}. Therefore, the results obtained in this experimental work are quite reasonable. All of the specimen types show similar crack behaviours (Fig. 8), and the disadvantages of delaminated interfaces and crack planes were universal to all specimens and should not affect the comparative study.

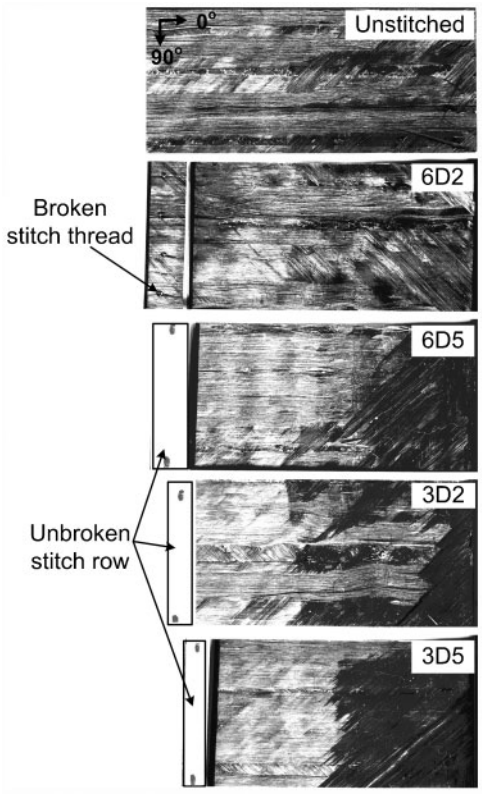

8 Crack propagation planes of all specimen types at pre-crack regions

Energy release rates

Each point of the G_{II} data has a specific value of slope m, as mentioned in equation (2). A typical C/Co versus $(a/L)^3$ curve is plotted in Fig. 9, and the slope m was calculated from this curve. Furthermore, G_{II} values were calculated, and R curves were plotted as shown in Fig. 10. In general, the unstitched and moderately stitched specimens presented similar R curves. The steady state regions (the flat regions) appeared for both unstitched and stitched laminates of 6 × 6 mm, 200 denier. To support this evidence, stitched specimens were cut into small pieces in between two stitched rows, so that one stitched row was present on each part, then separated slowly by hand. It was found that in the stitched sample of 6 × 6 mm 200 denier, the first and second rows of stitch threads were broken, as illustrated in Fig. 8. The maximum energy bridged by the stitch fibre was achieved, after which the energy release rate did not increase with further increases in the crack length. In stitched specimens of 6 × 6 mm 500 denier, no stitch fibre was broken, and the steady state zone was not obviously observed.

Furthermore, the densely stitched specimens showed desirable mode II delamination properties. Based on the cutting results described in Fig. 8, the stitch fibres were

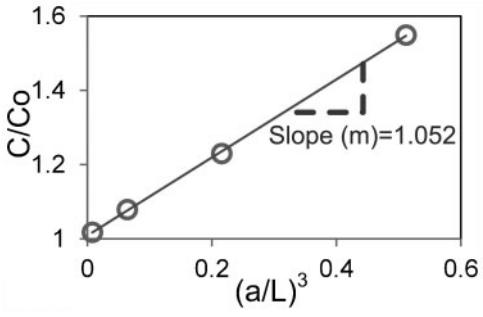

9 Typical specimen compliance curve in terms of *C/Co* versus $(a/L)^3$

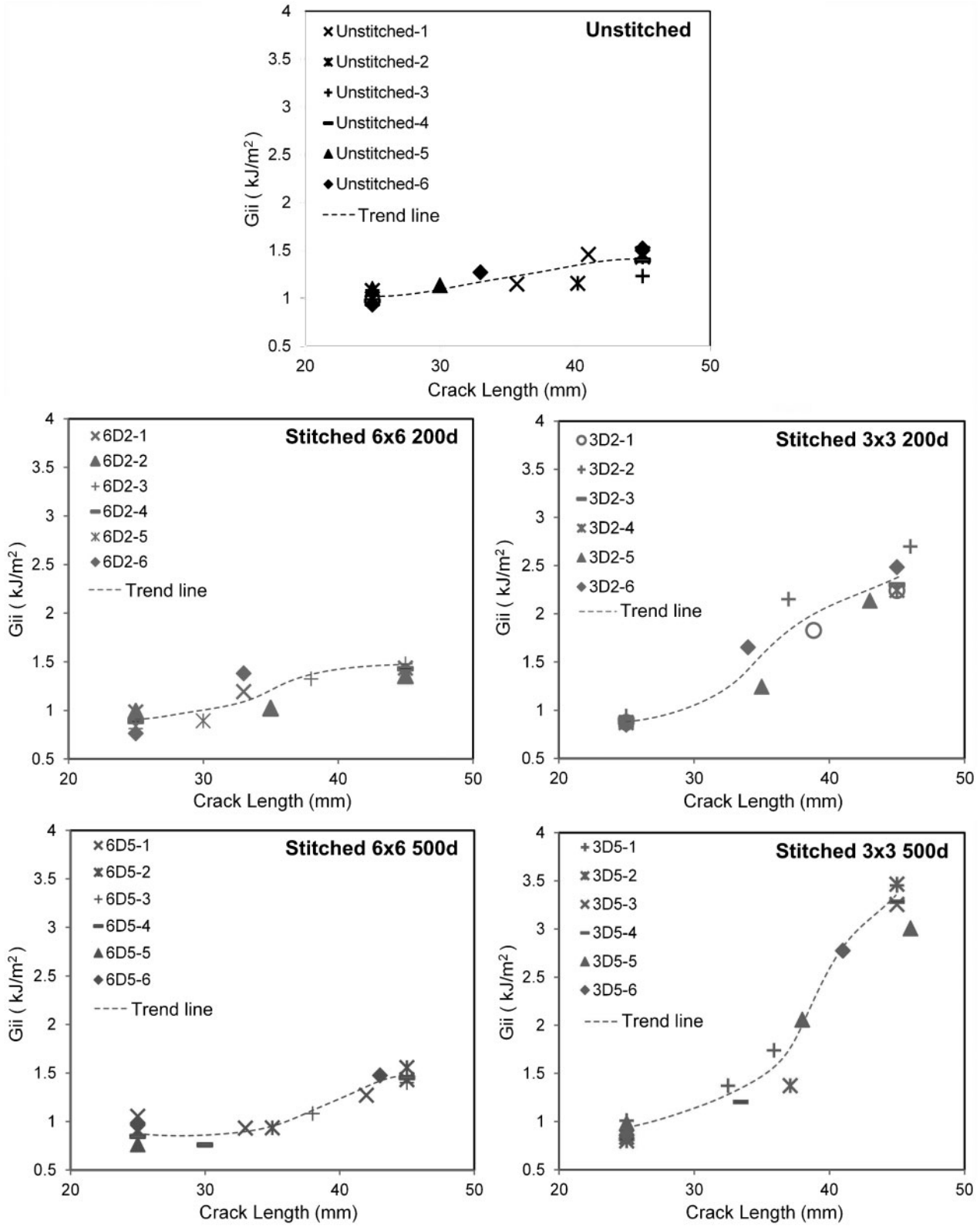

10 ***R*** **curves for unstitched and stitched specimens**

not broken during the test, so steady state regions were not attained.

To quantitatively evaluate the effect of stitching, the G_{IIC} values at the crack lengths a of 25 and 45 mm from each type of specimen are plotted in Fig. 11. It is worth noting that at a crack length of 25 mm, only one stitched row was present in the crack region, and it represented the crack tip was placed in the stitching environment (Fig. 2). Conversely, at a crack length of 45 mm, the crack region was fully stitched and the left overhang on Fig. 2 is only about 9–13 mm. There were, on average, eight and fifteen stitch rows in the crack zone for stitched specimens of 6×6 mm and 3×3 mm respectively.

At a crack length of 25 mm, all types of stitched specimens yielded lower G_{IIC} values (by ~13·4%) compared to the unstitched ones. One plausible reason

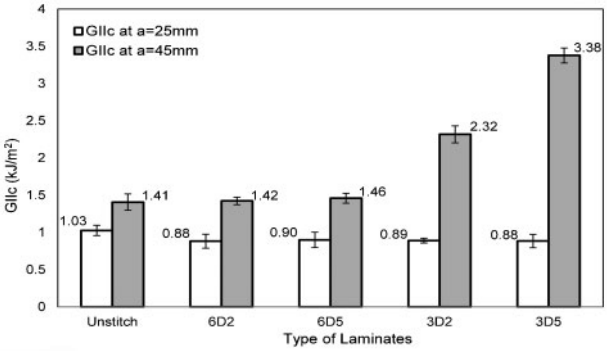

11 Average values of critical energy release rates G_{IIC} for crack lengths of 25 and 45 mm

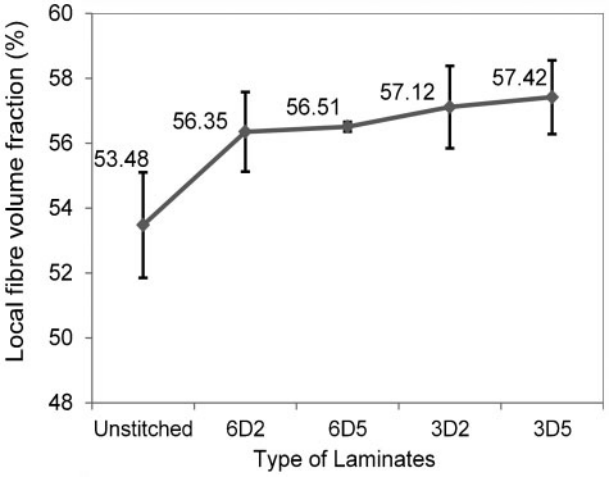

12 Local fibre volume fractions V_{fl} for each specimen type obtained by burnoff tests

why these G_{IIC} values were lower is that fibre compaction during the stitching process increased the local fibre volume fraction. A detailed explanation will be presented in the next section.

At a crack length of 45 mm, the moderately stitched specimens showed negligible increases in G_{IIC} compared to the unstitched ones (1·3 and 3·8% for specimens with stitched thread thicknesses of 200 and 500 denier respectively). Even though a certain amount of energy was absorbed by the stitch threads, G_{IIC} values were most affected by the stitching process itself, which reduced the G_{IIC} values as discussed above.

On the other hand, the densely stitched specimens underwent a significant improvement in G_{IIC} compared to the unstitched ones (64·8 and 140·3% increases for the specimens with stitch thread thicknesses of 200 and 500 denier respectively). In this case, the energy absorbed by the existence of the stitch threads significantly increased the G_{IIC} values.

Based on the above G_{IIC} data at crack lengths of 25 and 45 mm, particularly for densely stitched specimens, we recognise that the number of stitch threads at the crack area significantly determines the effectivity of delamination growth suppression. The G_{IIC} values at a crack length of 25 mm could be higher if more stitch threads are in the crack area. This issue could not be verified in more detail in this work due to the limited space available in the specimens. However, our group's previous work on damage progression of stitched composites under out of plane loading[39] could explain the delamination growth rate after small damage was initiated. In this case, the crack area was fully stitched (unlike in mode II specimens). It was observed that delamination growth in moderately stitched specimens was slightly slower than in unstitched ones, and delamination growth was suppressed significantly in densely stitched specimens.

The effect of stitch thread thickness is relatively small in the case of moderately stitched specimens (3%). In densely stitched specimens, thicker stitch threads (500 denier) exhibited G_{IIC} values that were 1·46 times those of thinner stitch threads (200 denier). This clearly showed that thicker stitch threads could absorb more energy during the test.

Fibre compaction effects

Local fibre volume fractions were plotted for each type of specimen (Fig. 12). Fibre compaction during the stitching process increased local fibre volume fractions by averages of 3 and 3·8% for moderately and densely stitched laminates respectively. These increments generate higher levels of maximum shear stress at the crack tip during ENF testing. Quantitatively, using the trend line in Fig. 4, these higher local fibre volume fractions could increase the maximum shear stress at the fibre/matrix interface around the crack tip by up to 9·9%. Furthermore, higher shear stresses around the crack tips allow for easier crack propagation and alleviate the values for G_{IIC} as reported previously.

Conclusions

Tabbed end notch flexural specimens exhibited a strong capability to prevent compression failure around a loading pin during mode II delamination tests. Thin aluminium tabs (1 mm in thickness) were enough to avoid plastic deformation and created a low shear stress at the tabs/laminate interface; hence, there was no tab debonding.

The test results revealed that low *SD* (2·78 cm^{-2}) affected G_{IIC} insignificantly. In this case, the energy absorbed by the stitch threads at the crack area was almost equal to the decreasing G_{IIC} values due to fibre compaction. Crack bridging due to stitch threads was significantly perceived for densely stitched specimens (*SD*, 11·11 cm^{-2}) with the increment of G_{IIC} reaching 2·4 times that of unstitched specimens. The effect of *SD* also could be observed from load–displacement curves, where in the unstitched and moderately stitched laminates, the load dropped drastically, but it did not drop in densely stitched laminates.

The effect of stitch thread thickness for moderately stitched specimens was relatively small (3%). However, for densely stitched laminates, specimens with a stitch thread thickness of 500 denier presented G_{IIC} values that were 1·5 times those of specimens with a stitch thread thickness of 200 denier.

Acknowledgements

The authors gratefully acknowledge Tokyo Metropolitan Government for its financial support from the Asian Human Resources Fund and Asian Network of Major Cities 21 (ANMC-21) Project. Special gratitude is extended to Professor L. A. Carlsson (Florida Atlantic University) for helpful discussion concerning the

compliance calibration method, Dr A. Yudhanto (currently at King Abdullah University of Science and Technology) for guidance during our stay at Tokyo Metropolitan University, Dr H. Hoshi (Japan Aerospace Exploration Agency) for valuable input on this work and Mr P. Joshi for correcting the language of this manuscript.

References

1. L. Tong, A. P. Mouritz and M. K. Bannister: 3D fibre reinforced polymer composites, Kidlington, Oxford, UK, 2002; Elsevier.
2. J. Ren, Y. K. Kim and J. Rice: *Text. Res. J.*, 2011, **81**, (4), 335–343.
3. A. P. Mouritz, C. Baini and I. Herszberg: *Composites A*, 1999, **30A**, 859–870.
4. Y. Tanzawa, N. Watanabe and T. Ishikawa: *Compos. Sci. Technol.*, 1999, **59**, (8), 1261–1270.
5. D. T. Fishpool, A. Rezai, D. Baker, S. L. Ogin and P. A. Smith: *Plast. Rubber Compos.*, 2013, **42**, (3), 108?114.
6. A. P. Mouritz: *Composites A*, 2007, **38A**, 2383–2397.
7. A. P. Mouritz and B. N. Cox: *Composites A*, 2000, **31A**, 1–27.
8. K. A. Dransfield, L. K. Jain and Y.-W. Mai: *Compos. Sci. Technol.*, 1998, **58**, 815–827.
9. M. D. K. Wood, X. Sun, L. Tong, A. Katzos, A. R. Rispler and Y.-W. Mai: *Compos. Sci. Technol.*, 2007, **67**, 1058–1072.
10. S. Solaimurugan and R. Velmurugan: *Compos. Sci. Technol.*, 2008, **68**, 1742–1752.
11. K. T. Tan, N. Watanabe, M. Sano, Y. Iwahori and H. Hoshi: *J. Compos. Mater.*, 2010, **44**, (26), 3203–3229.
12. M. F. S. F. De Moura: Delamination behaviour of composites, 310–326; 2008, Boca Raton, FL, CRC Press.
13. B. V. Sankar and S. K. Sharma: *Compos. Sci. Technol.*, 1997, **57**, 729–737.
14. L. K. Jain, K. A. Dransfield and Y.-W. Mai: *Compos. Sci. Technol.*, 1998, **58**, 829–837.
15. M. D. K. Wood, X. Sun, L. Tong, Q. Luo, A. Katzos and A. Rispler: *J. Compos. Mater.*, 2007, **41**, (14), 1743–1772.
16. K. T. Tan, N. Watanabe and Y. Iwahori: *J. Reinf. Plast. Compos.*, 2011, **30**, (2), 99–109.
17. Y. Yasui, F. Hori, M. Amano and J. Takeuchi: US patent no. 5,833,802, 1998, 1–12.
18. W. Hufenbach, A. Hornig, M. Gude, R. Böhm and F. Zahneisen: *Mater. Des.*, 2013, **50**, 839–845.
19. P. Davies, G. D. Sims, B. R. K. Blackman, A. J. Brunner, K. Kageyama, M. Hojo, K. Tanaka, G. Murri, C. Rousseau, B. Gieseke and R. H. Martin: *Plast. Rubber Compos.*, 1999, **28**, (9), 432–437.
20. A. J. Brunner, B. R. K. Blackman and P. Davies: *Eng. Fract. Mech.*, 2008, **75**, 2779–2794.
21. JIS K7086: Testing methods for interlaminar fracture toughness of carbon fibre reinforced plastics, Minato-ku, Tokyo, Japan, Japan Standard Association, 1993.
22. Hysol, Henkel Corporation. http://www.henkelna.com/product-search-1554.htm?nodeid=8797799809025 (accessed January 2014).
23. L. A. Carlsson and J. W. Gillespie: Mode-II interlaminar fracture of composites, Application of fracture mechanics to composite materials, Klaus Friedrich, AE Amsterdam, The Netherlands, 113–157; 1989, Elsevier Science Publisher.
24. B. R. K. Blackman, A. J. Brunner and J. G. Williams: *Eng. Fract. Mech.*, 2006, **73**, 2443–2455.
25. L. A. Carlsson, J. W. Gillespie and B. R. Trethewey: *Reinf. Plast. Compos.*, 1986, **5**, 170–187.
26. J. R. Reeder, K. Demarco and K. S. Whitley: *Composites A*, 2004, **35**, 1337–1344.
27. A. F. Gill, P. Robinson and S. Pinho: *Compos. Sci. Technol.*, 2009, **69**, 2368–2375.
28. V. Feret, H. Ghiasi and P. Hubert: *Appl. Compos. Mater.*, 2013, **20**, 415–429.
29. A. Yudhanto, N. Watanabe, Y. Iwahori and H. Hoshi: *Composites B* 2013, **46B**, 151–165.
30. M. Hojo, S. Matsuda, S. Ochiai, N. Tsujioka, Y. Nakanishi, Z. Maekawa and A. Murakami: *Adv. Compos. Mater.*, 2001, **10**, (2,3), 237–246.
31. S. M. Lee: *Mater. Sci.*, 1997, **32**, 1287–1295.
32. S.-Y. Fu, C.-Y. Yuea, X. Hua and Y.-W. Mai: *Compos. Sci. Technol.*, 2000, **60**, (4), 569–579.
33. JIS K7075: Testing methods for carbon fiber content and void content of carbon fiber reinforced plastics, Minato-ku, Tokyo, Japan, Japan Standard Association, 1991.
34. A. B. Pereira, A. B. De Morais, A. T. Marques and P. T. De Castro, *Compos. Sci. Technol.*, 2004, **64**, 1653–1659.
35. I. Chou, I. Kimpara, K. Kageyama and I. Ohsawa: ASTM STP 1230, American Society for Testing and Materials, Philadelphia, PA, USA, 1995, 132–151.
36. J. J. Polaha, B. D. Davidson, R. C. Hudson and A. Pieracci: *J. Reinf. Plast. Compos.*, 1996, **15**, 141–173.
37. A. B. De Morais: *Composites A*, 2004, **35A**, 51–57.
38. V. Mollón, J. Bonhomme, A. Argüelles and J. Viña: *Compos. Struct.*, 2012, **94**, 1187–1191.
39. K. T. Tan, A. Yoshimura, N. Watanabe, Y. Iwahori and T. Ishikawa: *Compos. Sci. Technol.*, 2013, **74**, 194–204.